inorganics

MDPI

Article

Elucidating the Structural Features of Bis(arylimino)acenaphthene (Aryl-BIAN) Bismuth Complexes: A Combined Single-Crystal X-ray Diffraction and Hirshfeld Analysis Approach

Beatriz P. Machado †, Maria Celador-Garcia †, Vitor Rosa * and Clara S. B. Gomes *

LAQV-REQUIMTE, Department of Chemistry, NOVA School of Science and Technology, NOVA University of Lisbon, 2829-516 Caparica, Portugal

* Correspondence: vitor.rosa@fct.unl.pt (V.R.); clara.gomes@fct.unl.pt (C.S.B.G.)

† These authors contributed equally to this work.

Abstract: Dimeric bismuth(III) complexes bearing bis(aryl-imino)acenaphthene (Aryl-BIAN) donor ligands of the general formulae [(Dipp-BIAN)$BiCl_3$]$_2$ **2**, [(*o*-*i*Pr-BIAN)$BiCl_3$]$_2$ **3**, and [(*p*-*i*Pr-BIAN)$BiCl_3$]$_2$ **4**, where Dipp = diisopropyl, *o*-*i*Pr = *ortho*-isopropyl and *p*-*i*Pr = *para*-isopropyl, were prepared by reaction of the corresponding neutral BIAN ligand with $BiCl_3$, under inert atmosphere conditions. X-ray studies were performed, and their molecular structures were determined. The individual contributions of intermolecular interactions to crystal packing have been quantified by means of Hirsfeld surface analysis.

Keywords: bismuth; bis(arylimino)acenaphthene (Aryl-BIAN) ligands; X-ray structure; Hirshfeld surface analysis

Citation: Machado, B.P.; Celador-Garcia, M.; Rosa, V.; Gomes, C.S.B. Elucidating the Structural Features of Bis(arylimino)acenaphthene (Aryl-BIAN) Bismuth Complexes: A Combined Single-Crystal X-ray Diffraction and Hirshfeld Analysis Approach. *Inorganics* **2024**, *12*, 135. https://doi.org/10.3390/inorganics12050135

Academic Editor: Wolfgang Linert

Received: 17 April 2024
Revised: 30 April 2024
Accepted: 2 May 2024
Published: 4 May 2024

1. Introduction

Bismuth is considered the heaviest stable element on the periodic table, and its remarkably low toxicity makes it a fascinating element for chemists [1]. It has relevance in various fields, including cosmetics, pigments, electronics, and pharmaceuticals (such as bibrocathol and bismuth subsalicylate), shown in Figure 1a,b, respectively [2]. This is due to its insolubility in neutral aqueous solutions, such as biological media [3].

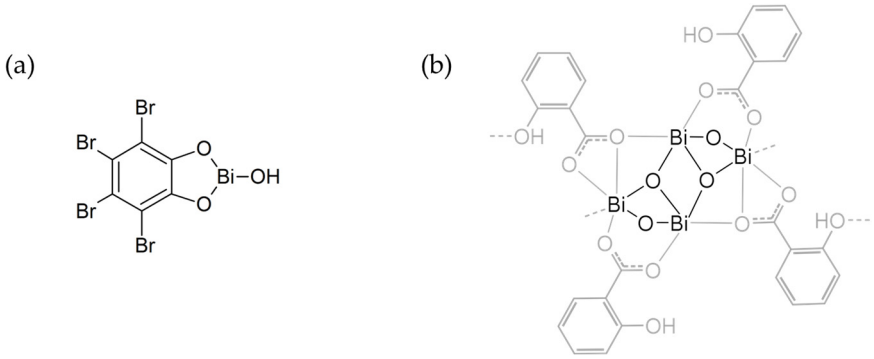

Figure 1. (**a**) Bibrocathol structure, commonly known as Posiformin, is used for controlling ocular infection swelling. (**b**) Bismuth subsalicylate, commonly known as Pepto-Bismol, is used to treat gastrointestinal diseases.

The +3-oxidation state of bismuth is the most dominant due to the presence of the inert pair effect. Additionally, Bi(III) compounds exhibit a potent soft Lewis acidity owing to the weak shielding of the 4f electrons [4]. This property makes it attractive for traditional homogenous catalysis, which relies on the activation of π-bonds or carbonyl compounds [5]. Bismuth is a promising element for coordination reactions, due to its ability to appear

in a variety of oxidation states, such as +5, which appears more often than +2 and +4 but is also known, and geometries depending on the coordination number that exhibits, including three, four, five, and seven, resulting in pyramidal, trigonal pyramidal, square-based pyramidal, and octahedral geometries [6,7]. It has been considered a promising element in redox processes, leading to potential applications in synthesis and catalysis. Bismuth complexes, such as Bi-Nb-O systems or $BiWO_6$, can be used as photocatalysts in different catalytic reactions [8,9]. Bismuth triflate can also be found in electroanalysis as modified electrodes or in organic reactions like Friedel–Crafts acylation, where it is used as a catalyst [10]. Bismuth also presents rich and diverse structural features, and when reacted with three-coordinating ligands, displays unique structural characteristics [11–13]. Evans et al**.** were even able to obtain stable tri-coordinated bismuth complexes after the abstraction of a chloride moiety [14–16]. It is worth noting that Bi complexes gain stability when one of the coordinating atoms is carbon.

Bis(arylimino) acenaphthene (Aryl-BIAN) ligands can enhance activity in certain systems due to their extensive **π**-system and rigid s-*cis* diimine unit, which can chelate to a metal center [17]. This ligand type is mainly relevant to late transition metals, such as palladium, nickel, copper, and zinc, for various organic transformations, including hydrogenation [18], ethylene polymerization [19,20], reverse atom transfer radical polymerization (ATRP) of styrene [21], click chemistry [22], selective oxidation of alcohols [23], and formation of cyclic carbonates [24].

Aryl-BIAN ligands have been employed to investigate complexes of Group 15 and 16, specifically phosphorus and arsenic complexes, for the formation of cyclic triphosphenium ions (Figure 2). Additionally, antimony complexes containing Aryl-BIAN ligands have been reported, demonstrating the utility of these ligands in supporting fluoro-, azido-, and cyano-antimony moieties. Hill et al. reported two bismuth complexes containing Aryl-BIAN ligands, [(Dipp-BIAN)$BiCl_3$] and [(Mes-BIAN)$BiCl_3$] (Mes = mesityl), in which the corresponding Aryl-BIAN reacted with $BiCl_3$ in equimolar quantities. The single-crystal X-ray diffraction of the [(Mes-BIAN)$BiCl_3$] complex revealed a ***μ***–Cl-bridged dimer, where the two Bi atoms are bridged by two Cl^- anions. The study of thallium(I), indium(III) [25], tin(IV), antimony (III), and bismuth (III) coordination complexes led to the conclusion that the solid-state structure adopted by each complex is determined by the nature of the metal atom and its ability to form donor–acceptor bonds, rather than the steric characteristics of the ligand [17,26,27].

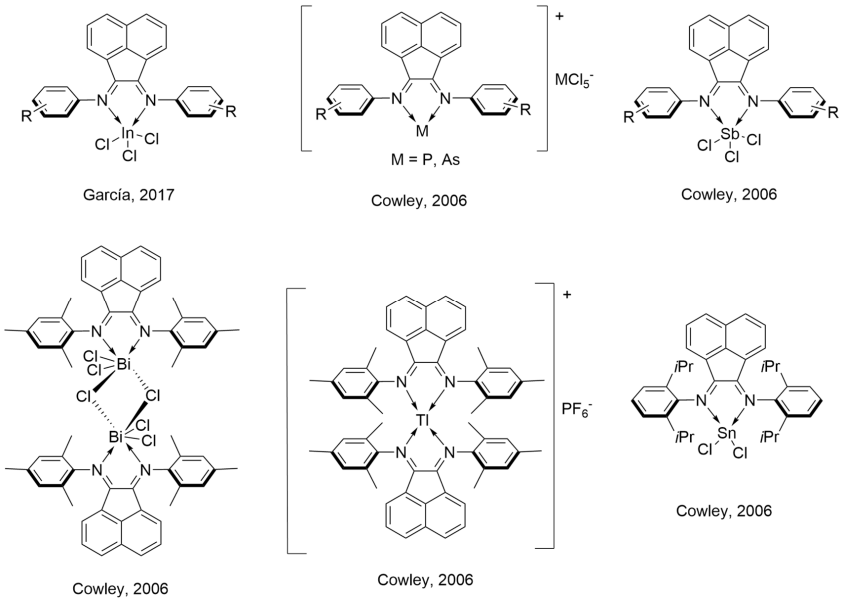

Figure 2. Reported heavy *p*-block complexes containing Ar-BIAN ligands [17,25].

This article focuses on X-ray crystal structures of bismuth complexes that contain known Aryl-BIAN ligands. Specifically, [(Dipp)$_2$BIAN]BiCl$_3$, [(*o*-*i*PrC$_6$H$_4$)$_2$BIAN]BiCl$_3$, and [(*p*-*i*PrC$_6$H$_4$)$_2$-BIAN]BiCl$_3$ were studied using single-crystal crystallography and Fourier Transform Infrared Spectroscopy (FTIR).

2. Results and Discussion

2.1. Synthesis and Characterization

The Aryl-BIAN ligands, (2,4,6-Me$_3$C$_6$H$_2$)$_2$BIAN (**L1**), (*o*,*o*′-*i*Pr$_2$C$_6$H$_3$)$_2$BIAN (**L2**), (*p*-*i*PrC$_6$H$_4$)$_2$BIAN (**L3**), and (*o*-*i*PrC$_6$H$_4$)$_2$BIAN (**L4**), where BIAN is bis(imino)acenaphthene, were prepared according to reported methods [28]. For **L1** and **L2**, the acid-catalyzed Schiff base reaction using an alcoholic solvent was used, whereas in the case of **L3** and **L4**, the template method using ZnCl$_2$ followed by demetallation assisted by potassium oxalate.

The synthesis of the Bi(III) complexes was carried out under inert atmosphere conditions in accordance with the procedure previously reported by Cowley and co-workers [17]. The expected Bi(III) complexes were afforded as orange–reddish solids, in moderate yields, by the addition of an equimolar amount of solid BiCl$_3$ to a solution of the corresponding Aryl-BIAN ligand in CH$_2$Cl$_2$, followed by stirring at room temperature for 16 h (Scheme 1). Crystals suitable for single crystal X-ray diffraction (see X-ray studies below) were obtained by recrystallization through solvent diffusion of pentane into a CH$_2$Cl$_2$ solution of the Bi(III) complexes. As observed and reported by Cowley and co-workers, all complexes were obtained in dimeric form [17].

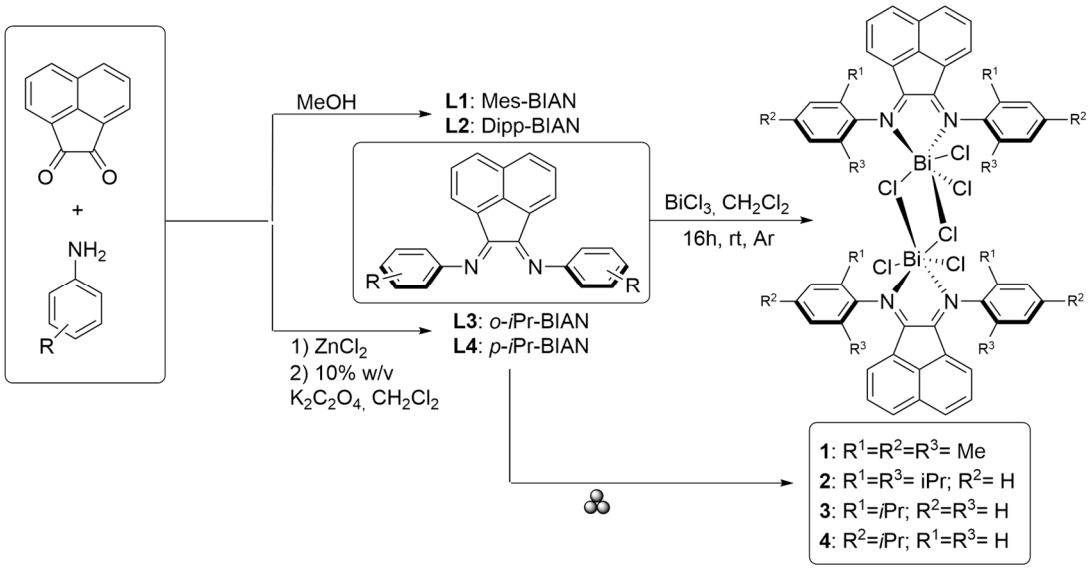

Scheme 1. Synthesis of Bi(III) complexes **1**–**4**.

These complexes were found to be poorly soluble in common laboratory solvents and proved to be very unstable both in solution and in the solid state, being extremely sensitive to moisture and oxygen atmosphere. In fact, they easily decomposed even under inert conditions. This sensitive nature was observed by X-ray diffraction studies. When analyzing a red crystalline sample of complex **3**, we observed the presence of colorless crystals mixed with red prisms. The nature of these colorless crystals was unambiguously established by single-crystal X-ray diffraction and corresponds to a salt (**3-decomposition**) with the general formula [(*o*-*i*Pr-C$_6$H$_4$NH$_3$)(BiCl$_4$)] (Scheme 2 and X-ray studies below).

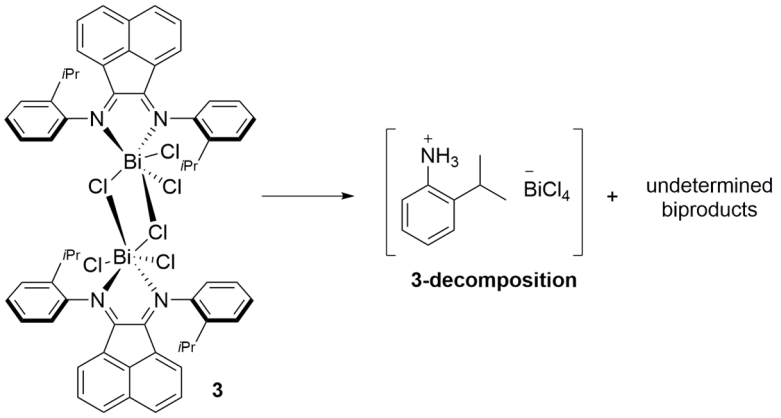

Scheme 2. Decomposition of complex **3**, leading to the formation of **3-decomposition**.

^{1}H NMR (proton Nuclear Magnetic Resonance) and FTIR spectroscopy were used to characterize these complexes, despite their propensity to decomposition. FTIR analysis was performed by comparing each complex's characteristic bands to its corresponding free ligand bands and bismuth salt. This proved that the complex was successfully formed, as a mixture of typical bands of each reagent appeared in the final product. Two typical bands of the bismuth salt were observed, one of which disappeared when coordinated to the ligand, which we presume to be water present in the compound, and the other at ca. 1575 cm^{-1}, which corresponds to the stretching of the Bi–Cl bond. This band is present in all complexes at 1581 cm^{-1} (**1**), 1585 cm^{-1} (**2**, **3**), and 1583 cm^{-1} (**4**). Additionally, the imine C=N band from the free ligand appears at approximately 1656 cm^{-1}. When coordinated to the bismuth, this band shifts to a lower wavelength number, confirming the formation of the complex. This band appears at 1624 cm^{-1} (**1**), 1621 cm^{-1} (**2**, **4**), and 1619 cm^{-1} (**3**). All spectra obtained are shown in Figures S1–S5 in the Supplementary Information (SI) section. The ^{1}H NMR spectra obtained showed more signals than expected, presumably due to the decomposition of the compound during the acquisition of the spectrum. However, comparison with the spectra of the free ligands confirms the formation of the expected bismuth complex. The acenaphthene backbone signals, defined by two duplets and a dd system, are present in all complexes with slight differences between the compounds. The main variations are observed in the *meta* protons of the aryl's groups of each complex. These variations are due to the presence of electron-donating groups (EDG) in the *ortho* and *para* positions. In addition, variations are present in the new bismuth complex spectra that have both *ortho* positions substituted. The *para*, *meta*, and *ortho* signals from these aryl groups are observed at 7.89 ppm, 7.36 ppm, and 6.60 ppm (**2**); 8.08 ppm, 7.49 ppm, and 6.99 ppm (**3**) and 8.02 ppm, 7.45 ppm, and 6.93 ppm, respectively. A slight downfield deviation was also observed when comparing the free ligand with the bismuth complex, indicating that the bismuth is acting as an electron-drawing group, decreasing the electron density, by deshielding the nucleus, and resulting in a larger chemical shift. All spectra obtained are shown in Figures S6–S9 in SI.

The formation of these dimeric Bi(III) complexes was also attempted by mechanochemistry for complex **3**. The first experiment was carried out in a planetary ball mill, under neat grinding conditions, for 1 h at 500 rpm. However, this resulted in an incomplete reaction in which a mixture of complex **3**, ligand **L3**, and $BiCl_3$ was observed. When the reaction was carried out using the same reaction conditions and milling parameters, but with a longer reaction time (2 h), complex **3** was obtained in quantitative yield.

2.2. X-ray Studies

Crystals suitable for single-crystal X-ray diffraction were obtained for derivatives **1**–**4** from solutions of dichloromethane double-layered with pentane. Their molecular structures are depicted in Figure 3, while their bond lengths, angles, and other relevant

structural parameters are displayed in Table 1. The molecular structure of complex **1** was in accordance with that previously reported in reference [17].

Complex **2** crystallized in the monoclinic system, *I*2/*a* space group, whereas complexes **3** and **4** crystallized in the triclinic system, in *P*−1 space group, as orange or red prisms. A representation of their morphology is presented in Figure 4.

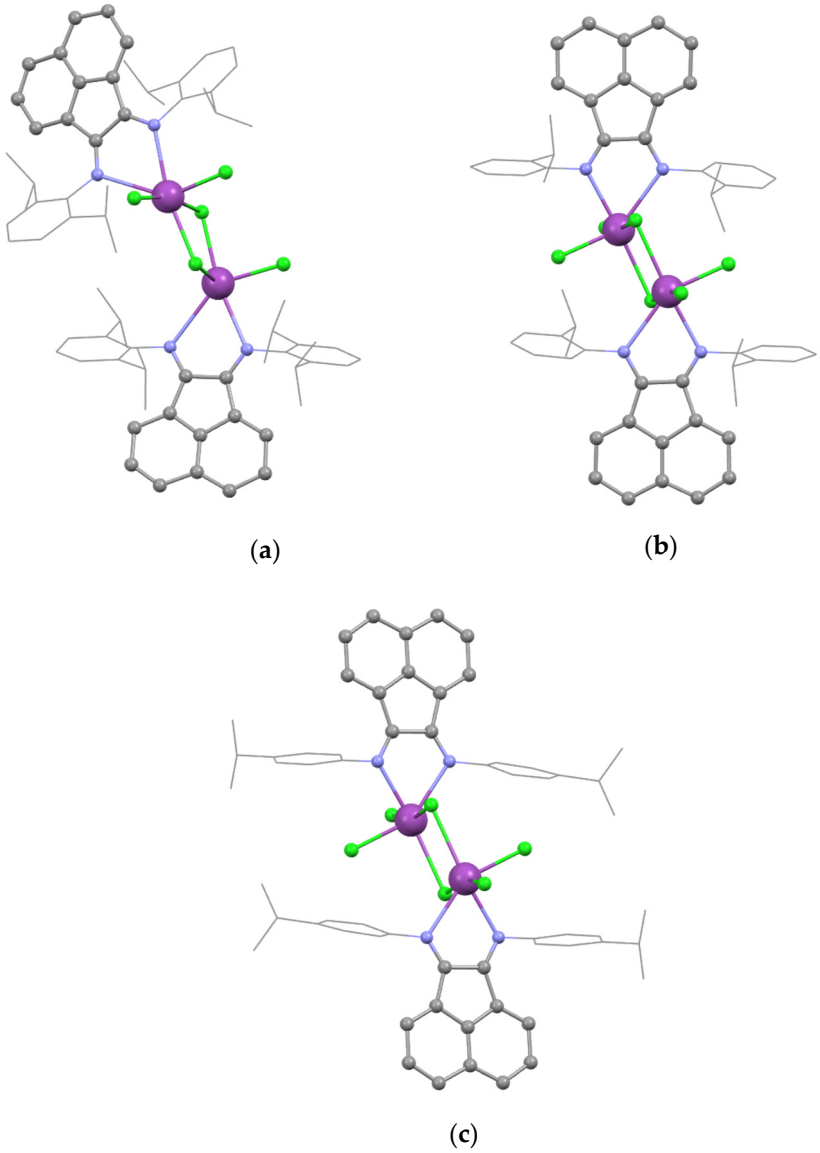

Figure 3. Mercury representations of the molecular structure of complexes (**a**) **2**, (**b**) **3**, and (**c**) **4**. All hydrogen atoms and a co-crystallized CH_2Cl_2 (in **4**) solvent molecule were omitted for clarity. Atom colors: grey—carbon, blue—nitrogen, green—chlorine, and purple—bismuth.

Table 1. Selected bond distances (Å) and angles (°), and other relevant structural parameters for compounds **2**, **3**, and **4**.

	2	**3**	**4**
Distances			
C1–N1	1.269 (12)	1.29 (3)	1.271 (7)
C11–N2	1.269 (11)	1.25 (3)	1.261 (7)
Bi1–N1	2.654 (8)	2.485 (19)	2.453 (5)
Bi1–N2	2.882 (7)	2.705 (16)	2.623 (5)

Table 1. *Cont.*

	2	3	4
Bi1–Cl1	2.465 (3)	2.551 (5)	2.760 (2)
Bi1–Cl2	2.493 (4)	2.837 (5)	2.4968 (17)
Bi1–Cl3	2.663 (3)	2.475 (5)	2.5844 (19)
Bi1–Cl# [a]	3.143 (3)	2.829 (5)	2.9642 (19)
Angles			
N1–Bi1–N2	61.3 (2)	64.7 (5)	66.03 (14)
Cl1–Bi1–Cl3	87.21 (10)	95.49 (18)	164.63 (6)
Cl2–Bi1–Cl1	93.92 (13)	95.54 (17)	94.45 (8)
Cl2–Bi1–Cl3	91.46 (11)	90.40 (16)	92.10 (8)
N1–Bi1–Cl3	168.8 (2)	148.0 (4)	165.00 (12)
N2–Bi1–Cl2	143.19 (16)	176.2 (4)	150.98 (11)
ω [b]	9.3 (5)	10.5 (3)	19.9 (3)
φ_1 [c]	93.7 (3)	71.1 (5)	89.99 (15)
φ_2 [c]	88.2 (3)	77.8 (5)	70.7 (3)

[a] Cl#—atom generated by a symmetry operation. [b] Dihedral angle between planes of the aryl rings. [c] Dihedral angle between the plane of the acenaphthene and those of the aryl rings.

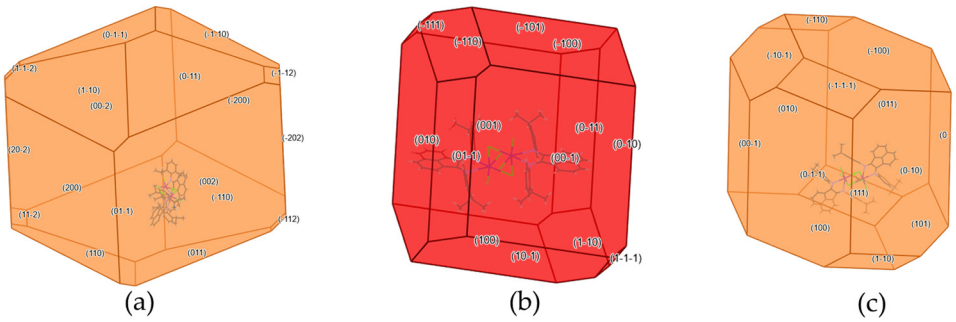

Figure 4. Mercury representations of the morphology of complexes (**a**) **2**, (**b**) **3**, and (**c**) **4**.

As depicted in Figure 3, all complexes have the molecular structure of a μ^2–chloride-bridged dimer, with only a half molecule in their asymmetric units. In the case of complex **4**, a co-crystallized dichloromethane molecule is also present in the asymmetric unit. Within the dimeric species, each bismuth center is coordinated to a [N,N] donor set of the Aryl-BIAN ligand and four chlorine atoms, resulting in a hexacoordinated bismuth atom. The degree of distortion can be assessed by analyzing the bond angles around the metal center. For a pure octahedral geometry, the angles between *cis*-coordinating positions should be 90°, whereas those between ligands in *trans* positions should be 180°. As can be seen in Table 1, the bond angles around the Bi(III) atom deviate slightly from the ideal 90 and 180 º, confirming that complexes **2**–**4** have a distorted octahedral geometry around each Bi(III) center. The Bi–N bond distances, which vary between 2.453 (5) and 2.882 (7) Å, show a certain degree of asymmetry. The larger bond length, 2.882 (7) Å in complex **2**, is still much smaller than the sum of the van der Waals radii for Bi and N (3.85 Å). This asymmetry and the longer Bi–N bond lengths are much more pronounced in the derivatives containing substituents in the *ortho* position (complexes **2** and **3**). Furthermore, these Bi–N bond lengths, especially those observed for **2**, are longer than those observed for related mono- and binuclear neutral Aryl-BIAN–Bi(III) complexes (2.648 (5) and 2.540 (5) Å [29] and 2.606 (2) and 2.708 (2) Å [17]), or in other bismuth complexes bearing related N,N-donor ligands, such as phenanthroline [$(phen)_2BiCl_3$] (2.456 and 2.548 (31) Å) [30] or bipyridine [$(bipy)BiBr_3$] (2.417 and 2.516 Å) [31]. An analysis of the bond distances of the chloride bridges (Table 1) shows a remarkable asymmetry in complex **2**, with very long bond distances of 2.663 (3) and 3.143 (3) Å, respectively. This asymmetry is slightly lower in complex **4** and absent in complex **3**, as the difference in the bond distances is within the s.u. of the bond length.

Further analysis to the conformation adopted by these Bi(III) complexes (Figure 3 and Table 1) reveals that in all complexes the dihedral angle ω, which is related to the relative position of the two aryl substituents, is very small, varying between 9.3 (5) and 19.9 (3)°. This indicates that the aryl rings of the BIAN ligands are almost coplanar in the solid-state structure. Additionally, the angle φ (dihedral angle between the acenaphthene backbone and the aryl rings) is also a relevant parameter, providing important information on the relative conformation of the aryl substituents with respect to the rigid BIAN moiety. The observed values in Table 1 show that, in complex **2**, the aryl rings are perfectly perpendicular to the acenaphthene backbone due to the presence of the *o*,*o*′-isopropyl substituents, which impose some rigidity to the structure and hinder the rotation around the N–C_{ipso} bond. In contrast, in complexes **3** and **4**, the aryl rings show a certain degree of distortion, deviating from perpendicularity.

The 3D-supramolecular arrangement in complexes **2**, **3**, and **4** is generated by intermolecular interactions of the type C–H. . .Cl, C–H. . .π, and π . . .π (Figures S10, S12, and S14 and Table 2).

Table 2. Intermolecular interactions in complexes **2**, **3**, and **4**.

Complex	D–H. . .A	H. . .A	D. . .A	D–H. . .A	Symmetry Operation
2	C33–H33A. . . π	2.93	3.560 (13)	145	½-*x*, *y*, 1-*z*
	C28–H28. . .Cl1	2.83	3.644 (13)	144	*x*, 1 + *y*, *z*
3	C7–H7. . .Cl1	2.89	3.748 (3)	117	2-*x*, 1-*y*, 2-*z*
	C26–H26. . .Cl1	2.85	3.730 (3)	152	2-*x*, -*y*, 2-*z*
	C17–H17. . .π	2.88	3.724 (3)	108	1-*x*, 1-*y*, 1-*z*
	π . . .π		3.40 (3)	101.9 (15)	2-*x*, 1-*y*, 2-*z*
4	C8–H8. . .Cl2	2.80	3.576 (8)	142	−1 + *x*, *y*, -*z*
	C31–H31A. . .Cl3	2.74	3.635 (13)	154	2-*x*, 1-*y*, 1-*z*
	C5–H5. . .Cl5	2.95	3.684 (3)	137	1-*x*, 1-*y*, 2-*z*

As mentioned above, during the X-ray studies of complex **3**, we observed a mixture of red and colorless prisms. The crystal structure of these colorless prisms has been unequivocally determined by single crystal X-ray diffraction, showing that they are the decomposition product of complex **3** upon exposure to moisture and oxygen, a salt with the general formula [(*o*-*i*Pr-$C_6H_4NH_3$)($BiCl_4$)] (**3-decomposition**). Its molecular structure is depicted in Figure 5, with selected bond distances (Å) and angles (°) in the respective figure caption.

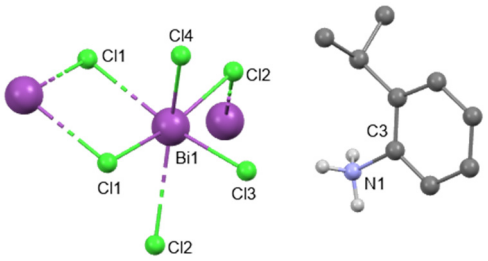

Figure 5. Mercury representations of the molecular structure of compound **3-decomposition**. All hydrogen atoms were omitted for clarity. Atom colors: grey—carbon, blue—nitrogen, white—hydrogen, green—chlorine, and purple—bismuth. Selected bond distances (Å): C3–N1 1.509 (11), Bi1–Cl1 2.783 (3), Bi1–Cl2 2.624 (3), Bi1–Cl3 2.608 (3), Bi1–Cl4 2.531 (3), Bi1–Cl1# 2.880 (3), and Bi1–Cl2 3.162 (3). Selected bond angles (°): Cl1–Bi1–Cl2 164.37 (9), Cl1–Bi1–Cl3 86.92 (8), Cl1–Bi1–Cl4 79.18 (9), Cl3–Bi1–Cl2 92.38 (8), and Cl3–Bi1–Cl1# 163.41 (9). Atom generated by a symmetry operation.

This compound crystallized in the monoclinic system, $P2_1/c$ space group, with a cation and an anion in the asymmetric unit. The molecular structure of compound **3-decomposition** consists of a protonated aniline, as the cation, and $BiCl_4^-$ as the bismuth

anion. Interestingly, the bismuth anion is actually a polymeric structure where the two remaining coordination positions are generated by the symmetry operations 1-*x*, 1-*y*, 2-*z*, and 1-*x*, ½ + *y*, 1.5-*z* (Figure S16), although the molecular formula of the anion is defined as $BiCl_4^-$. Consequently, the total coordination number around the Bi(III) center is six, resulting in a distorted octahedral geometry. In addition, the supramolecular arrangement of compound **3-decomposition**, when viewed along the *b*-axis, shows 1D chains of the bismuth anion intercalated by two rows of cations oriented in opposite directions.

2.3. Hirshfeld Surface Analysis

Hirshfeld surfaces have been used as a useful approach to the visualization of intermolecular interactions and the quantification of their individual contribution to crystal packing. Figure 6 is an example of a 3D surface plot of the d_{norm} property for complex **3**. The corresponding Hirshfeld surfaces for complexes **2** and **4** are shown in Figures S17 and S18. The bright and intense red spots on the Hirshfeld surface (Figure 6) indicate strong intermolecular interactions, such as C–H. . .Cl short contacts.

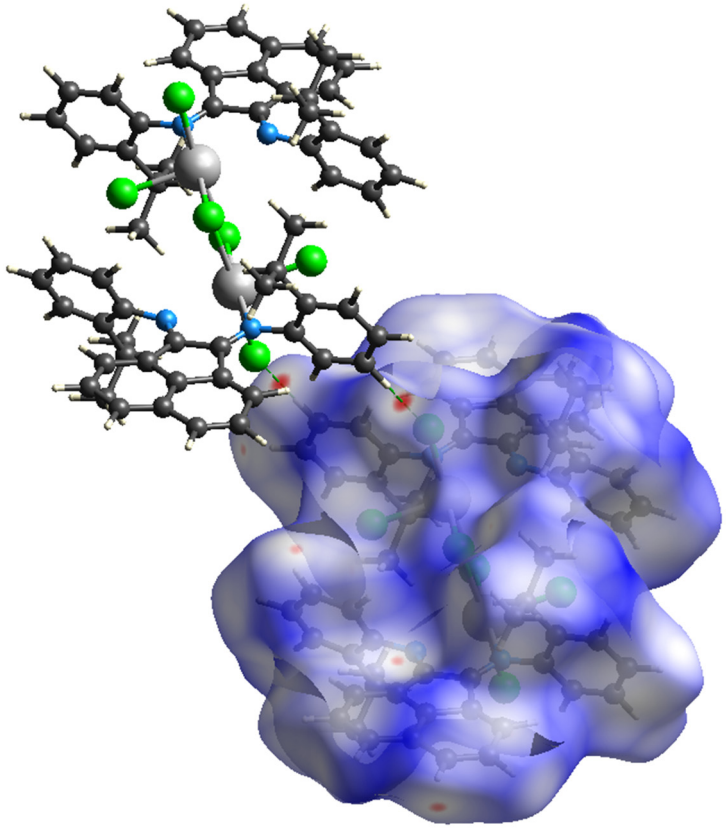

Figure 6. 3D Hirshfeld surface for complex **3**, mapped with d_{norm} properties, showing intermolecular C–H. . .Cl contacts (green dashed lines).

To highlight the individual contribution of the relevant intermolecular contacts, the 2D fingerprint plots (d_i versus d_e) were plotted for all complexes and are shown in Figures S19–S21. As can be seen, the H. . .H contacts are the most important contributors to the total Hirshfeld surface area for all complexes, with a total percentage of 65.9%, 60.4%, and 45.1% for complexes **2**, **3**, and **4**, respectively (Figure S22). The small van der Waals radii of the hydrogen atom explain this high percentage, since H. . .H contacts have the shortest distance on the surface. However, they do not appear as intense red spots on the d_{norm} surface because the normalized H. . .H contact distances are usually larger than the other contacts, such as H. . .Cl/Cl. . .H or H. . .C(π)/C(π). . .H. The second most important interaction in all derivatives is H. . .Cl/Cl. . .H, with a total percentage of 19.9% (**2**),

17.5% (**3**), and 34.3% (**4**). This higher value for complex **4** can be explained by the absence of substituents on the *ortho* positions of the aryl rings. In the case of complexes **2** and **3**, the presence of *o*,*o*′-diisopropyl and *o*-isopropyl substituents may hinder some of these interactions. Finally, interactions between hydrogen and carbon atoms, especially π bonds, are the third most important intermolecular interactions. This represents 12.3%, 18.5%, and 13.3% of the total intermolecular interactions for complexes **2**, **3**, and **4**, respectively. These observations agree with those obtained experimentally using X-ray crystallography.

3. Materials and Methods

3.1. General Considerations

All reactions were carried out using Schlenk techniques under an argon atmosphere with the use of dry solvents, unless otherwise specified. Diethyl ether and pentane were dried over metallic sodium prior to distillation under argon. Dichloromethane was dried over calcium hydride prior to distillation.

Ligands Mes-BIAN (**L1**), Dipp-BIAN (**L2**), (*o*-*i*PrC_6H_4)$_2$BIAN (**L3**), (*p*-*i*PrC_6H_4)$_2$BIAN (**L4**) [28], and [(Mes)$_2$BIAN]$BiCl_3$ **(1)** [17] were synthesized following reported methodology and characterization corresponded to the described data.

Infrared (IR) spectra were acquired in a FT-IR Spectrum Two (Perkin-Elmer) in Attenuated Total Reflectance (ATR) mode.

Nuclear Magnetic Resonance (NMR) spectra were recorded using a Bruker Avance III 400 MHz or 500 MHz spectrometer (Germany), with probe QNP 100 MHZ S1 with Z-gradient and processed with the TOPSPIN 3.2 software (Bruker). Spectra were referenced internally using the residual protio solvent resonance relative to tetramethylsilane ($\delta = 0$). Multiplicities were abbreviated as follows: doublet (d), triplet (t), quintet (p), and multiplet (m).

3.2. Synthetic Procedures

The general procedure for synthesizing the complexes involves adding the corresponding ligand (1 eq) to a solution of $BiCl_3$ (1 eq) in CH_2Cl_2, which was previously dried using Schlenk techniques and allowing it to react for 16 h. The resulting solution was then filtered through celite. To obtain crystals suitable for single-crystal X-ray diffraction, the solution was concentrated and then a dichloromethane/pentane double layer was made to induce precipitation by slow diffusion.

Synthesis of **[(Dipp-BIAN)$_2$BiCl$_3$]** (**2**): A solution of Dipp-BIAN (**L1**) (200 mg, 0.4 mmol) in CH_2Cl_2 (20 mL) was prepared, and then solid $BiCl_3$ was added (125 mg, 0.4 mmol), obtaining an orange-colored powder yielding 11% (69.3 mg). ^{1}H NMR (400 MHz, $CDCl_3$) δ (ppm): 7.89 (d, J = 8.2 Hz, 2H), 7.36 (t, J = 7.7 Hz, 2H), 7.21 (d, J = 9.4 Hz, 4H), 7.16–7.09 (m, 2H), 6.60 (d, J = 7.1 Hz, 2H), 2.99 (p, J = 6.9 Hz, 4H), 1.22 (d, J = 6.7 Hz, 12H), and 0.92 (d, J = 6.8 Hz, 12H). FTIR-ATR (cm^{-1}): 2964 (C=C), 1621 (C=N), and 1585 (Bi-Cl).

Synthesis of **[(*o*-*i*PrC$_6$H$_4$)$_2$-BIAN)BiCl$_3$]** (**3**): A solution of (*o*-*i*PrC_6H_4-BIAN) (**L2**) (166 mg; 0.4 mmol) in CH_2Cl_2 (20 mL) was prepared, and then solid $BiCl_3$ was added (125 mg, 0.4 mmol). A red solid was recovered that yielded 37% (216.3 mg). ^{1}H NMR (400 MHz, $CDCl_3$) δ (ppm): 8.08 (d, J = 8.4 Hz, 2H), 7.49 (t, J = 8.0 Hz, 2H), 7.43 (d, J = 8.7 Hz, 4H), 7.16 (d, J = 8.0 Hz, 2H), 6.99 (d, J = 7.1 Hz, 2H), 3.03 (p, J = 6.9 Hz, 2H), and 1.33 (d, J = 6.9 Hz, 14H). FTIR-ATR (cm−1): 2967 (C=C), 1619 (C=N), and 1585 (Bi-Cl).

Synthesis of **[(*p*-*i*PrC$_6$H$_4$)$_2$-BIAN)BiCl$_3$]** (**4**): A solution of (*p*-*i*PrC_6H_4-BIAN) (166 mg; 0.4 mmol) in CH_2Cl_2 (20 mL) was prepared, and then solid $BiCl_3$ was added (125 mg; 0.4 mmol). A bright orange-colored powder was recovered yielding 36% (206.8 mg). ^{1}H NMR (400 MHz, $CDCl_3$) δ (ppm): 8.02 (d, J = 8.3 Hz, 2H), 7.45 (t, J = 7.8 Hz, 2H), 7.38 (d, J = 8.2 Hz, 4H), 7.33–7.28 (m, 4H), 6.93 (d, J = 7.3 Hz, 2H), 3.02 (p, J = 6.9 Hz, 2H), and 1.33 (d, J = 6.9 Hz, 12H). ^{13}C NMR (101 MHz, $CDCl_3$) δ (ppm): 159.3 (C=N), 146.3 (C-N), 131.3, 131.2, 129.3, 128.0, 127.83, 127.4, 124.2, 123.7, 118.5, 33.9 ($CH(CH_3)_2$), and 24.4 (CH_3). FTIR-ATR (cm^{-1}): 2957 (C=C), 1621 (C=N), and 1583 (Bi-Cl).

3.3. X-ray Diffraction

Single crystals of complexes **2**, **3, 3-decomposition**, and **4** were selected, covered with Fomblin (polyfluoro-ether oil) and mounted on a nylon loop. Experimental details are presented in Table 3. The data were collected at 293 K on a Bruker D8 Venture diffractometer equipped with a Photon II detector, using graphite monochromated Mo-Kα radiation (λ = 0.71073 Å). The data were processed using the APEX4 suite software package, which includes integration and scaling (SAINT), absorption corrections (SADABS) [32], and space group determination (XPREP). Structure solution and refinement were carried out using direct methods with the programs SHELXT 2018/2 and SHELXL (version 2019/2) [33] inbuilt in APEX, and WinGX-Version 2023.1 [34] software packages. All non-hydrogen atoms were refined anisotropically. All hydrogen atoms were inserted in idealized positions and allowed to refine riding on the parent carbon with fixed 1.2 Ueq of their parent carbon atom or 1.5 Ueq for the methyl group. The crystals of **2** and **3** were of poorer quality and showed low diffracting power, exhibiting dynamic motion or thermal disorder that was impossible to solve. Nevertheless, all atoms were correctly assigned and in agreement with the results obtained by other characterization techniques. The molecular diagrams were drawn with Mercury [35]. The data were deposited in the Cambridge Crystallographic Data Centre (CCDC) under deposit numbers 2344653 for **2**, 2344654 for **3**, 2344655 for **3-decomposition**, and 2344656 for **4**.

Table 3. Crystallographic data and details about refinement for structures **2**, **3, 3-decomposition**, and **4**.

	2	**3**	**3-decomposition**	**4**
Formula	$C_{36}H_{40}BiCl_3N_2$	$C_{60}H_{56}Bi_2Cl_6N_4$	$C_{18}H_{28}Bi_2Cl_8N_2$	$C_{62}H_{60}Bi_2Cl_{10}N_4$
M	816.05	1463.74	973.98	1633.60
λ (Å)	0.71073	0.71073	0.71073	0.71073
T (K)	293 (2)	293 (2)	293 (2)	293 (2)
Crystal system	Monoclinic	Triclinic	Monoclinic	Triclinic
Space group	$I\,2/a$	$P\,-1$	$P\,2_1/c$	$P\,-1$
a (Å)	23.176 (12)	10.539 (5)	16.076 (5)	11.9071 (19)
b (Å)	12.210 (5)	11.459 (5)	7.1593 (18)	12.515 (2)
c (Å)	28.154 (12)	12.812 (6)	12.799 (3)	12.836 (2)
α (°)	90	95.385 (19)	90	62.832 (6)
β (°)	98.17 (4)	113.799 (16)	105.698 (11)	75.498 (6)
γ (°)	90	98.125 (18)	90	89.515 (7)
V (Å^3)	7886 (6)	1382.0 (12)	1418.1 (6)	1635.0 (5)
Z	8	1	2	1
ρ_{calc} (g.cm^{-3})	1.375	1.759	2.281	1.659
μ (mm^{-1})	4.698	6.691	13.157	5.823
Crystal size	0.30 × 0.20 × 0.16	0.20 × 0.20 × 0.16	0.30 × 0.26 × 0.20	0.30 × 0.16 × 0.12
Crystal color	Orange	Red	Colorless	Orange
Crystal description	Prism	Prism	Prism	Prism
θ_{max} (°)	25.347	25.970	27.614	28.968
Total data	56725	36055	19467	91864
Unique data	7180	5348	3244	8389
R_{int}	0.2648	0.2080	0.1552	0.1158
R [$I > 2\sigma(I)$]	0.0788	0.1083	0.0581	0.0519
R_w	0.1860	0.2627	0.1340	0.1065
Goodness of fit	1.019	1.065	1.037	1.101
ρ_{min}	−1.639	−3.817	−3.987	−1.226
ρ_{max}	2.509	9.817	3.855	2.019

3.4. Hirschfield Surface Analysis

The evaluation of the intermolecular interactions present in the crystal structure has been carried out by the Hirshfeld surfaces analysis [36,37]. Any electron density inside the isosurface is mainly due to the contribution of the molecules under consideration, whereas the electron density outside the surface is dominated by the rest of the crystal

lattice components. The property d_{norm} consists of two parameters defining the distance of an atom from the isosurface: d_i, when the atom is inside the surface, and d_e, when the atom is outside [38]. This property has been mapped onto the Hirshfeld surface, providing a visual representation of the strength of the contacts across the molecule using a color scale. Strong intermolecular interactions, characterized by short contacts, are shown as intense red areas on the Hirshfeld surface, indicating areas where the value of d_{norm} is negative and the sum of d_i and d_e is less than the sum of the van der Waals radii. Conversely, the weakest interactions, with long contacts, are represented by blue color, passing through white for intermediate interactions. The Hirshfeld surfaces in the crystal lattices were calculated using the *CrystalExplorer* software [39], which gives an indication of the crystal packing and the strength of the intermolecular forces in the lattices. Furthermore, all points on the Hirshfeld surface were also plotted as 2D fingerprints [40], which establish a correlation between d_e and d_i, which correspond to the distances to the nearest outer and inner atoms, respectively. The color of the 2D plot also indicates the density of points in the region. Red represents a high number of interactions corresponding to this [d_e,d_i] region, and the color changes from blue to green as the density of points decreases. Information about the type, density, and strength of the interactions is provided by the fingerprint plots.

4. Conclusions

Three new bismuth complexes with different Aryl-BIAN substitutions were synthesized and characterized using ^{1}H NMR and FTIR spectroscopy. The complexes were found to be sensitive and decomposed during analysis. One of the subproducts of such decomposition was isolated for the first time, allowing a more in-depth knowledge of its behavior, specifically when the ligands present an imine function. Single-crystal diffraction studies revealed that coordination occurred through N–Bi donor–acceptor bonds, resulting in a hexacoordinated bismuth atom with a distorted octahedral geometry. The 3D supramolecular arrangement analysis allowed for the study of the main interactions present in the complexes, including C–H. . .Cl, C–H. . .π, and π. . .π. The Hirshfeld surface analysis was primarily used to quantify the individual contributions of the intermolecular interactions to crystal packing. It was concluded that the H. . .H interactions were the most significant.

Supplementary Materials: The following supporting information can be downloaded at: https://www.mdpi.com/article/10.3390/inorganics12050135/s1—Supplementary Information and CIF file containing compounds **2**, **3**, **4**, and **3-decomposition**.

Author Contributions: Conceptualization: C.S.B.G. and V.R.; methodology: C.S.B.G. and V.R.; formal analysis: B.P.M., M.C.-G., C.S.B.G. and V.R.; investigation: B.P.M. and M.C.-G.; writing—original draft preparation: B.P.M. and C.S.B.G.; writing—review and editing: C.S.B.G. and V.R.; supervision: C.S.B.G. and V.R. All authors have read and agreed to the published version of the manuscript.

Funding: This work received financial support from the Fundação para a Ciência e Tecnologia (FCT) through projects UIDB/50006/2020 (https://doi.org/10.54499/UIDB/50006/2020, accessed on 16 April 2024), UIDP/50006/2020 (https://doi.org/10.54499/UIDP/50006/2020, accessed on 16 April 2024), and LA/P/0008/2020 (https://doi.org/10.54499/LA/P/0008/2020, accessed on 16 April 2024).

Data Availability Statement: Data are contained within the article and Supplementary Material. CIF files can be obtained free of charge from the Cambridge Crystallographic Data Centre (CCDC) at https://www.ccdc.cam.ac.uk/, accessed on 16 April 2024.

Acknowledgments: C. S. B. Gomes acknowledges the XTAL—Macromolecular Crystallography group (UCIBIO and i4HB) for granting access to the X-ray diffractometer and the X-ray infrastructure (RECI/BBBBEP/0124/2012).

Conflicts of Interest: The authors declare no conflicts of interest.

References

1. de Marcillac, P.; Coron, N.; Dambier, G.; Leblanc, J.; Moalic, J.-P. Experimental Detection of α-Particles from the Radioactive Decay of Natural Bismuth. *Nature* **2003**, *422*, 876–878. [CrossRef] [PubMed]

2. Mato, M.; Cornella, J. Bismuth in Radical Chemistry and Catalysis. *Angew. Chem. Int. Ed.* **2024**, *63*, e202315046. [CrossRef] [PubMed]
3. Yang, Y.; Ouyang, R.; Xu, L.; Guo, N.; Li, W.; Feng, K.; Ouyang, L.; Yang, Z.; Zhou, S.; Miao, Y. Review: Bismuth Complexes: Synthesis and Applications in Biomedicine. *J. Coord. Chem.* **2015**, *68*, 379–397. [CrossRef]
4. Berger, R.J.F.; Rettenwander, D.; Spirk, S.; Wolf, C.; Patzschke, M.; Ertl, M.; Monkowius, U.; Mitzel, N.W. Relativistic Effects in Triphenylbismuth and Their Influence on Molecular Structure and Spectroscopic Properties. *Phys. Chem. Chem. Phys.* **2012**, *14*, 15520–15524. [CrossRef] [PubMed]
5. Lichtenberg, C. Bismuth-Based Lewis Acidity. In *Advances in Inorganic Chemistry*; Meyer, K., van Eldik, R., Eds.; Elsevier: Amsterdam, The Netherlands, 2023; Volume 82, pp. 237–260, ISBN 9780443159442.
6. Yukhin, Y.M.; Daminov, A.S.; Logutenko, O.A.; Koledova, E.S.; Mishchenko, K.V. Processing of Metallic Bismuth for the Production of Bismuth Compounds. *Sep. Sci. Technol.* **2021**, *56*, 1168–1176. [CrossRef]
7. Sadler, P.J.; Li, H.; Sun, H. Coordination Chemistry of Metals in Medicine: Target Sites for Bismuth. *Coord. Chem. Rev.* **1999**, *185–186*, 689–709. [CrossRef]
8. Zhang, N.; Ciriminna, R.; Pagliaro, M.; Xu, Y.-J. Nanochemistry-Derived Bi_2WO_6 Nanostructures: Towards Production of Sustainable Chemicals and Fuels Induced by Visible Light. *Chem. Soc. Rev.* **2014**, *43*, 5276–5287. [CrossRef] [PubMed]
9. Zhai, H.; Shang, S.; Zheng, L.; Li, P.; Li, H.; Luo, H.; Kong, J. Efficient Visible-Light Photocatalytic Properties in Low-Temperature Bi-Nb-O System Photocatalysts. *Nanoscale Res. Lett.* **2016**, *11*, 383. [CrossRef] [PubMed]
10. Ollevier, T. New Trends in Bismuth-Catalyzed Synthetic Transformations. *Org. Biomol. Chem.* **2013**, *11*, 2740–2755. [CrossRef]
11. Kindervater, M.B.; Marczenko, K.M.; Werner-Zwanziger, U.; Chitnis, S.S. A Redox-Confused Bismuth(I/III) Triamide with a T-Shaped Planar Ground State. *Angew. Chem. Int. Ed.* **2019**, *58*, 7850–7855. [CrossRef]
12. Tidwell, J.R.; Martin, C.D. Investigating the Reactions of $BiCl_3$, a Diiminopyridine Ligand, and Trimethylsilyl Trifluoromethanesulfonate. *Organometallics* **2022**, *41*, 1197–1203. [CrossRef]
13. Šimon, P.; del Proft, F.; Jambor, R.; Růžička, A.; Dostál, L. Monomeric Organoantimony(I) and Organobismuth(I) Compounds Stabilized by an NCN Chelating Ligand: Syntheses and Structures. *Angew. Chem. Int. Ed.* **2010**, *49*, 5468–5471. [CrossRef] [PubMed]
14. Kindra, D.R.; Casely, I.J.; Fieser, M.E.; Ziller, J.W.; Furche, F.; Evans, W.J. Insertion of CO_2 and COS into Bi–C Bonds: Reactivity of a Bismuth NCN Pincer Complex of an Oxyaryl Dianionic Ligand, [2,6-$(Me_2NCH_2)_2C_6H_3$]Bi($C_6H_2{}^tBu_2O$). *J. Am. Chem. Soc.* **2013**, *135*, 7777–7787. [CrossRef] [PubMed]
15. Casely, I.J.; Ziller, J.W.; Fang, M.; Furche, F.; Evans, W.J. Facile Bismuth−Oxygen Bond Cleavage, C−H Activation, and Formation of a Monodentate Carbon-Bound Oxyaryl Dianion, $(C_6H_2{}^tBu_2$-3,5-O-4$)^{2-}$. *J. Am. Chem. Soc.* **2011**, *133*, 5244–5247. [CrossRef] [PubMed]
16. Kindra, D.R.; Evans, W.J. Bismuth-Based Cyclic Synthesis of 3,5-Di-Tert-Butyl-4-Hydroxybenzoic Acid via the Oxyarylcarboxy Dianion, $(O_2CC_6H_2{}^tBu_2O)^{2-}$. *Dalton Trans.* **2014**, *43*, 3052–3054. [CrossRef] [PubMed]
17. Hill, N.J.; Reeske, G.; Moore, J.A.; Cowley, A.H. Complexes of 1,2-Bis(Aryl-Imino)Acenaphthene (Ar-BIAN) Ligands with Some Heavy p-Block Elements. *Dalton Trans.* **2006**, *40*, 4838–4844. [CrossRef] [PubMed]
18. Kluwer, A.M.; Koblenz, T.S.; Jonischkeit, T.; Woelk, K.; Elsevier, C.J. Kinetic and Spectroscopic Studies of the [Palladium(Ar-Bian)]-Catalyzed Semi-Hydrogenation of 4-Octyne. *J. Am. Chem. Soc.* **2005**, *127*, 15470–15480. [CrossRef]
19. Camacho, D.H.; Salo, E.V.; Ziller, J.W.; Guan, Z. Cyclophane-Based Highly Active Late-Transition-Metal Catalysts for Ethylene Polymerization. *Angew. Chem.* **2004**, *116*, 1857–1861. [CrossRef]
20. Gomes, C.S.B.; Ribeiro, A.F.G.; Fernandes, A.C.; Bento, A.; Rosário Ribeiro, M.; Kociok-Köhn, G.; Pascu, S.I.; Duarte, M.T.; Gomes, P.T. Reactivity of Cationic α-Diimine Cyclopentadienyl Nickel Complexes towards $AlEt_2Cl$: Synthesis, Characterisation and Ethylene Polymerisation. *Catal. Sci. Technol.* **2017**, *7*, 3128–3142. [CrossRef]
21. Fliedel, C.; Rosa, V.; Santos, C.I.M.; Gonzalez, P.J.; Almeida, R.M.; Gomes, C.S.B.; Gomes, P.T.; Lemos, M.A.N.D.A.; Aullón, G.; Welter, R.; et al. Copper(II) Complexes of Bis(Aryl-Imino)Acenaphthene Ligands: Synthesis, Structure, DFT Studies and Evaluation in Reverse ATRP of Styrene. *Dalton Trans.* **2014**, *43*, 13041. [CrossRef]
22. Viana, M.S.; Gomes, C.S.B.; Rosa, V. Heteroleptic Copper Complexes as Catalysts for the CuAAC Reaction: Counter-Ion Influence in Catalyst Efficiency. *Catalysts* **2023**, *13*, 386. [CrossRef]
23. Rosa, V.; Laronha, H.; Gomes, C.S.B.; Cordas, C.M.; Brinco, J.; Freitas, F.; Gomes da Silva, M.D.R.; Avilés, T. Aerobic Oxidation of Benzylic Alcohols Catalysed by New (Aryl-BIAN)Copper(I) Complexes: Their Synthesis and Structural Characterization. *Appl. Organomet. Chem.* **2023**, *37*, e7193. [CrossRef]
24. Zakrzewska, M.E.; André, P.J.L.; Gomes, C.S.B.; Nunes, A.V.M.; Rosa, V. Zinc Complexes Bearing BIAN Ligands as Efficient Catalysts for the Formation of Cyclic Carbonates from CO_2 and Epoxides. *New J. Chem.* **2023**, *47*, 6551–6562. [CrossRef]
25. Wang, J.; Ganguly, R.; Yongxin, L.; Díaz, J.; Soo, H.S.; García, F. Synthesis and the Optical and Electrochemical Properties of Indium(III) Bis(Arylimino)Acenaphthene Complexes. *Inorg. Chem.* **2017**, *56*, 7811–7820. [CrossRef] [PubMed]
26. Wang, J.; Soo, H.S.; Garcia, F. Synthesis, Properties, and Catalysis of p-Block Complexes Supported by Bis(Arylimino)Acenaphthene Ligands. *Commun. Chem.* **2020**, *3*, 113. [CrossRef] [PubMed]
27. Reeske, G.; Hoberg, C.R.; Hill, N.J.; Cowley, A.H. Capture of Phosphorus(I) and Arsenic(I) Moieties by a 1,2-Bis(Arylimino) Acenaphthene (Aryl-BIAN) Ligand. A Case of Intramolecular Charge Transfer [*J. Am. Chem. Soc.* **2006**, *128*, 2800−2801]. *J. Am. Chem. Soc.* **2006**, *128*, 5300. [CrossRef]

28. van Asselt, R.; Elsevier, C.J.; Smeets, W.J.J.; Spek, A.L.; Benedix, R. Synthesis and Characterization of Rigid Bidentate Nitrogen Ligands and Some Examples of Coordination to Divalent Palladium. X-ray Crystal Structures of Bis (*p*-tolylimino) Acenaphthene and Methylchloro [Bis(*o*,*o*′-diisopropylphenyl-imino) Acenaphthene] Palladium (II). *Recl. Trav. Chim. Pays-Bas* **1994**, *113*, 88–98. [CrossRef]
29. Brazeau, A.L.; Jones, N.D.; Ragogna, P.J. Chemistry of the Heavy Group 15 Elements with the Pyridyl Tethered 1,2-Bis(Imino)Acenaphthene "Clamshell" Ligand. *Dalton Trans.* **2012**, *41*, 7890–7896. [CrossRef] [PubMed]
30. Bowmaker, G.A.; Hannaway, F.M.M.; Junk, P.C.; Lee, A.M.; Skelton, B.W.; White, A.H. Synthetic, Structural and Vibrational Spectroscopic Studies in Bismuth(III) Halide/N,N′-Aromatic Bidentate Base Systems. V Bismuth(III) Halide/N,N′-Bidentate Ligand (1:2) Systems. *Aust. J. Chem.* **1998**, *51*, 331–336. [CrossRef]
31. Bowmaker, G.A.; Hannaway, F.M.M.; Junk, P.C.; Lee, A.M.; Skelton, B.W.; White, A.H. Synthetic, Structural and Vibrational Spectroscopic Studies in Bismuth(III) Halide/N,N′-Aromatic Bidentate Base Systems. IV Bismuth(III) Halide/N,N′-Bidentate Ligand (1:1) Systems. *Aust. J. Chem.* **1998**, *51*, 325–330. [CrossRef]
32. Krause, L.; Herbst-Irmer, R.; Sheldrick, G.M.; Stalke, D. Comparison of Silver and Molybdenum Microfocus X-ray Sources for Single-Crystal Structure Determination. *J. Appl. Crystallogr.* **2015**, *48*, 3–10. [CrossRef] [PubMed]
33. Sheldrick, G.M. Crystal Structure Refinement with SHELXL. *Acta Crystallogr. C Struct. Chem.* **2015**, *71*, 3–8. [CrossRef] [PubMed]
34. Farrugia, L.J. WinGX and ORTEP for Windows: An Update. *J. Appl. Crystallogr.* **2012**, *45*, 849–854. [CrossRef]
35. MacRae, C.F.; Sovago, I.; Cottrell, S.J.; Galek, P.T.A.; McCabe, P.; Pidcock, E.; Platings, M.; Shields, G.P.; Stevens, J.S.; Towler, M.; et al. Mercury 4.0: From Visualization to Analysis, Design and Prediction. *J. Appl. Crystallogr.* **2020**, *53*, 226–235. [CrossRef] [PubMed]
36. Spackman, M.A.; Jayatilaka, D. Hirshfeld Surface Analysis. *CrystEngComm* **2009**, *11*, 19–32. [CrossRef]
37. Milin, E.; Benaicha, B.; El Hajj, F.; Patinec, V.; Triki, S.; Marchivie, M.; Gómez-García, C.J.; Pillet, S. Magnetic Bistability in Macrocycle-Based Fe^{II} Spin-Crossover Complexes: Counter Ion and Solvent Effects. *Eur. J. Inorg. Chem.* **2016**, *2016*, 5305–5314. [CrossRef]
38. McKinnon, J.J.; Jayatilaka, D.; Spackman, M.A. Towards Quantitative Analysis of Intermolecular Interactions with Hirshfeld Surfaces. *Chem. Commun.* **2007**, *7*, 3814–3816. [CrossRef]
39. Spackman, P.R.; Turner, M.J.; McKinnon, J.J.; Wolff, S.K.; Grimwood, D.J.; Jayatilaka, D.; Spackman, M.A. *CrystalExplorer*: A Program for Hirshfeld Surface Analysis, Visualization and Quantitative Analysis of Molecular Crystals. *J. Appl. Crystallogr.* **2021**, *54*, 1006–1011. [CrossRef]
40. Spackman, M.A.; McKinnon, J.J. Fingerprinting Intermolecular Interactions in Molecular Crystals. *CrystEngComm* **2002**, *4*, 378–392. [CrossRef]